


Effect of milling time on electrochemical properties of $\text{CaNi}_{4.8}\text{Mg}_{0.2}$ anode material of Ni-MH battery

Imen Karaoud¹, Youssef Dabaki^{1,2} , Yassine Ben Belgacem¹, Chokri Khaldi¹, Omar ElKedim³, Nouredine Fenineche⁴, Jilani Lamloumi¹

¹ Université de Tunis, ENSIT, LR99ES05, 1008 Montfleury, Tunisia

² Laboratoire de Physico-Chimie de l'Atmosphère (LPCA), Université du Littoral Côte d'Opale (ULCO), EA 4493, 59140 Dunkerque, France

³ FEMTO-ST, MN2S, UTBM, UBFC, 90010 Belfort Cedex, France.

⁴ ICB-PMDM/FR FCLAB, UTBM, UBFC, 90010 Belfort Cedex, France

Correspondence

Youssef Dabaki, Université de Tunis, ENSIT, LR99ES05, 1008 Montfleury, Tunisia & Laboratoire de Physico-Chimie de l'Atmosphère (LPCA), Université du Littoral Côte d'Opale (ULCO), EA 4493, 59140 Dunkerque, France

Email: dabakiyoussef@gmail.com

Abstract The objective of this study is to investigate the effect of milling time on the structural, morphological, and electrochemical properties of $\text{CaNi}_{4.8}\text{Mg}_{0.2}$ type alloy which is used as a negative electrode of Ni-MH batteries. The $\text{CaNi}_{4.8}\text{Mg}_{0.2}$ alloys are synthesized by mechano-synthesis using a Retsch PM400 ball mill for different milling times of 30, 40, 50, and 60 hours, using a ball-to-powder weight to a ratio of 8:1, under an argon atmosphere. The electrochemical properties are studied with different methods such as galvanostatic polarization and potentiodynamic polarization, at ambient temperature and in 6M KOH electrolyte. The highest discharge capacity, the highest reversibility as well as good kinetics are observed for the $\text{CaNi}_{4.8}\text{Mg}_{0.2}$ alloy with a milling time of 30h.

Keywords $\text{CaNi}_{4.8}\text{Mg}_{0.2}$ type alloy, Mechanical alloying, Battery Ni-MH, Electrochemical polarization technique

1. Introduction

Electronic devices have become common place and rapidly consumed, including laptops, electric vehicles, and cell phones (Ref 1,2). Therefore, the demand for rechargeable batteries is increasing. In addition, increasing air pollution and stricter emission standards for combustion vehicles are contributing to a growing interest in electric and hybrid vehicles (Ref 3,4). To meet these new demands, modern batteries must be efficient, economical, safe, lightweight, and environmentally friendly (Ref 5). Until now, despite various innovations, including lead acid, nickel-cadmium, and lithium-ion batteries, none of them has been able to fully meet these requirements (Ref 6-10). As a result of these limitations and the increasing demands on batteries, nickel-metal hydride batteries (Ni-MH) have been developed and commercialized since the 1990s (Ref 11,12). Ni-MH (Nickel Metal Hydride) battery has become the most dominant battery due to several advantages such as good charge-discharge capacity, long lifetime, and no negative effects on the environment (Ref 13,15). It is now a key component for advanced information and telecommunications systems and the next generation of hybrid or fully electric vehicles (Ref 16,17). In fact, the performance of this type of battery relies not only on the performance of the active materials (the type of hydrogen storage alloys) (Ref 18) but also on the production procedure of the negative electrodes, because, it influences charge/discharge properties (Ref 19). Several methods of elaboration are used, citing as examples, arc melting (Ref 20), induction melting (Ref 21), and mechanosynthesis (Ref 22). Focus on the mechanosynthesis methods or mechanical alloying is a common method for synthesizing and improving the hydrogen storage properties of the metal hydride (Ref 23-25). It is a very high-energy milling technique that consists in mixing and combining powders in the solid state and reducing the size of the particles to obtain homogeneous powders (Ref 26,27).

During milling, the powder particles are trapped between balls or one ball and the vial surface, and thanks to the energy provided by the mill the particles are milled (Ref 28). The milling process involves the optimization of several variables to find the desired product phase or microstructure, such as milling speed, milling time, ball/powder weight ratio, milling atmosphere, etc. It has several advantages compared to other methods, such as easy and controlled synthesis, simple and not expensive method that operate at room temperature (Ref 29). Metal hydrides were used in rechargeable batteries for hydrogen storage (Ref 30). It is characterized by several properties, such as hydrogen storage capacity, hydrogen absorption/desorption plateau pressure, thermodynamic and kinetic properties, activation and deactivation, etc (Ref 31). The hydrogen atom is stored in the solid material at the interstitial position (Ref 32). The principal hydrogen storage compounds are AB₅ (Ref 33,34), AB₃ (Ref 35,36), AB₂ (Ref 37,38), AB (Ref 39,40), and A₂B₇ (Ref 41,42). The AB₅ type is the most popular and studied because of its advantages. The crystal structure of the metal compound AB₅ was determined in 1942 by Nowotny and confirmed in 1959 by Wernick and Geller (Ref 43). It crystallizes in the hexagonal structure of the CaCu₅ type in the space group P6/mmm (Ref 44,45). Indeed, it has, generally, a storage capacity of about 1.5 wt%, using the solid-gas method, in near-ambient conditions (ambient temperature and low atmospheric pressure) (Ref 46), which signifies a high reactivity with hydrogen. Its electrochemical discharge capacity can achieve a maximum value of 370 mAhg⁻¹, in addition to its ease of activation (Ref 47,48). This family is also characterized by the facility of substitution of compounds A and B by other elements (Ref 49). Indeed, A is usually lanthanum which may be partially or totally substituted by Yttrium (Y) (Ref 50), Calcium (Ca) (Ref 51), Mischmetal (Mm) (Ref 52), Cerium (Ce) (Ref 53), Zirconium (Zr) (Ref 54). B is frequently nickel that can be substituted by transition

elements that are extremely (Ref 55) varied such as Aluminum (Al) (Ref 56), Manganese (Mn) (Ref 57), Zinc (Zn) (Ref 58), Tin (Sn) (Ref 59), Fer (Fe) (Ref 60), and Cobalt (Co) (Ref 61). Hydrogenation properties of LaNi_5 of AB_5 type were first discovered in the Philips Eindhoven laboratory (Ref 62). The rare-earth compound LaNi_5 , of the AB_5 family, could absorb up to 6 H/u.f at room temperature under a pressure of 2 bars and then desorb this hydrogen (Ref 63). In order to improve the absorption properties, a substitution can be made in the base alloy of other elements, either to "A" or to "B" (Ref 64-66). Several compositions have been studied and the best results, in terms of electrochemical performance, have been obtained with the $\text{LaNi}_{3.55}\text{Mn}_{0.4}\text{Al}_{0.3}\text{Co}_{0.75}$ compound. A. Merzouki et al. (Ref 67) made a comparative study of the compounds $\text{LaNi}_{3.55}\text{Mn}_{0.4}\text{Al}_{0.3}\text{Co}_{0.75}$, LaNi_5 , and its mono-substituted derivatives. They found that the tri-substituted compound $\text{LaNi}_{3.55}\text{Mn}_{0.4}\text{Al}_{0.3}\text{Co}_{0.75}$ was the best-performing compound in terms of stability and lifetime. In fact, the cost of Lanthanum material (La) is relatively expensive, so it can be completely replaced by calcium (Ca). In addition to that, the CaNi_5 compound has a theoretical discharge capacity of 482 mAhg^{-1} which is higher than that of LaNi_5 (372 mAhg^{-1}), so it is possible to improve the performance of LaNi_5 metal hydride by replacing Lanthanum with Calcium (Ref 68). The CaNi_5 compound has high electrochemical discharge capacity but limited cyclic stability (Ref 69). For this reason, some attempts have been made to improve the hydrogen storage properties of CaNi_5 by partially substituting Ca and/or Ni with other elements. J.O. Jensen et al. (Ref 70) studied the effect of the substitution of Ni in the basic compound CaNi_5 by different metals (Al, Cr, Mn, Co, Fe, Cu, Zn, Sn, and Mg) for two substitution rates $x=0.5$ and 1. They found that all the electrodes are easily activated. Only the $\text{CaNi}_{5-x}\text{M}_x$ ($\text{M} = \text{Cu, Zn, and Mg}$) electrodes preserved the same discharge capacity of CaNi_5 . The $\text{CaNi}_{5-x}\text{M}_x$ ($\text{M} = \text{Zn and Mg}$) electrodes had several cycles with a

capacity of 100 mAhg^{-1} higher than that of CaNi_5 , therefore, they present higher stability than that of CaNi_5 . Partial substitution of the nickel by other elements is always expected in order to maintain the main advantageous characteristics such as high electrochemical discharge capacity, good cyclic stability, long self-discharge, efficient catalytic properties, fast diffusion of atomic hydrogen through the lattice, appropriate H_2 equilibrium pressure, acceptable corrosion, resistance, long lifetime (Ref 71,72). G.liang et al. (Ref 73) investigated the influence of partial substitution of CaNi_5 by Mm, Zn, and Al on the electrochemical properties. They showed that the combination of the substitution of Ca by Mm and Ni by Zn and Al significantly improves the stability of the electrode. However, the substitution of Zn and Al does not protect the electrode from degradation and leads to a reduction in capacity. S. Chumphongphan et al. (Ref 74) made a comparison of the hydrogen storage properties of $\text{CaNi}_{5-x}\text{M}_x$ (M=Mo, Al) compounds for $x=0.1$ and 0.2 compared to the CaNi_5 base compound. Indeed, all the electrodes have higher maximum discharge capacities than CaNi_5 . But the cycling stability is improved only for the $\text{CaNi}_{4.9}\text{Al}_{0.1}$ electrode. Y. Dabaki et al. (Ref 75,76) have extensively studied the compound $\text{CaNi}_{5-x}\text{Mn}_x$ ($x=0.3, 0.5, 1$) elaborated by mechanosynthesis for different milling times (2, 10, 20, 30, 40, 50, 60h). The electrochemical results indicate that for the three substitutions $x=0.3, 0.5, 1$, the maximum discharge capacity is found for a milling time of 40h, which are, respectively, 125, 119, 109 mAhg^{-1} .

Within the same framework and based on a previous study (Ref 77) focused on the $\text{CaNi}_{4.8}\text{Mg}_{0.2}$ compounds prepared for 40h of mechanical milling and 8:1 ball-to-powder weight ratio, our investigation will extend to analyze the structural, morphological, and electrochemical properties of $\text{CaNi}_{4.8}\text{Mg}_{0.2}$ compounds for different milling times 30, 40, 50, and 60 h.

2. Experimental

2.1 Synthesis and characterization of CaNi_{4.8}Mg_{0.2} powders milled during 30, 40, 50, and 60h

Mechanical alloying is a technique for processing homogeneous powdered materials by mechanical processes based on the fractionation of particles by shock. It is used to produce powder's various morphologies and sizes up to tens of nanometers and to create more active sites for the penetration of hydrogen (Ref 78). The CaNi_{4.8}Mg_{0.2} powders are produced by the mechanosynthesis method using a Retsch PM400 high-energy planetary ball mill with an angular speed of 400 rpm, for different milling times (30, 40, 50, and 60h) at a ball-to-powder weight ratio of 8:1, in an argon atmosphere and at room temperature. After the synthesis of the powders, structural and morphological characterizations are performed using, respectively, Bruker D8 Advance XRD with $\text{Co}\alpha$ radiation ($\lambda = 1.789 \text{ \AA}$) and scanning electron microscope SEM JEOL JSM -5800LV.

2.2 Electrochemical characterization of CaNi_{4.8}Mg_{0.2} (30, 40, 50, 60h) electrodes

2.2.2 Preparation of the working electrode and the electrochemical cell

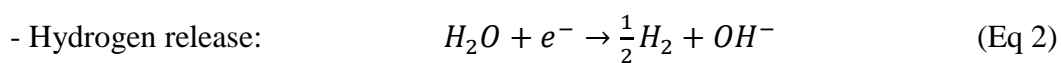
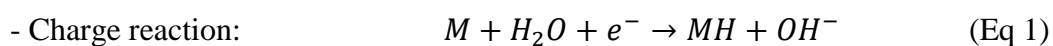
The electrochemical characterization of the CaNi_{4.8}Mg_{0.2} (30, 40, 50, 60 h) negative electrodes is carried out using the electrochemical device Galvanostat-Potentiostat Ec-Lab system (BiologicTM). An electrochemical cell is connected to this experimental device through its three electrodes; a working electrode (negative electrode), an auxiliary electrode (positive electrode) formed by a coiled nickel wire to increase its surface, and a reference electrode (Hg/HgO) filled with potassium that is used to measure its potential. All electrodes are immersed in a 6M KOH electrolyte. The metal hydride electrode (working electrode) is prepared using a so-called 'Latex' technique (Ref 79,80). Firstly, 90% of the alloy powder is mixed with 5% of carbon black in order to increase the electronic conductivity of the electrode and 5% of fine particles

of polytetrafluoroethylene (PTFE) act as a mechanical binder to give elasticity to the electrode. Secondly, the whole mixture is wetted with a few of ethanol and agitated until a paste is obtained, which is spread with a glass roller several times until the alcohol evaporates and a paste is obtained (latex) (Ref 81). Finally, after drying under vacuum for 24 hours at room temperature, the "Latex" formed is cut to the required size and then compressed on both sides of the nickel grid, acting as a current collector, to 0.5 cm² each to form the working electrodes. The wire providing the electrical contact is made of nickel.

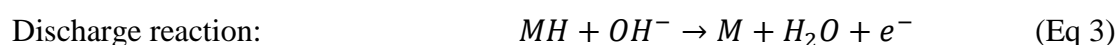
2.2.3 The different electrochemical characterization techniques

Galvanostatic polarization is the imposition of a constant current between the working electrode and the auxiliary electrode during charging and discharging to measure the potential between the working electrode and the reference electrode as a function of time.

The true charge capacity is not experimentally accessible because the cell is open and therefore it is impossible to determine the quantity of monoatomic hydrogen inserted into the negative electrode which is competitive with the quantity of hydrogen gas released.



During discharge, no outgassing is observed and therefore the capacity measurement can be performed.



By using the chronopotentiograms, we can determine the discharge capacity for each cycle during a long cycling, by the following equation:

$$C_{th}(mAh/g) = i(mA) \cdot \frac{t(h)}{m(g)} \quad (\text{Eq 4})$$

m: Mass of alloy contained in the negative electrode (g),

i: Discharge current (mA),

t: Discharge time (h).

Potentiodynamic polarization is based on the application of a potential E_{app} to the working electrode compared to the reference electrode that varies linearly with time from an initial potential, $E_i = -0.6$ V, to a final potential, $E_f = -1.3$ V, or vice versa, with a potential sweep rate, $v = 1 \text{ mVs}^{-1}$, according to the equation $E_{app} = \pm vt + E_i$ (Eq 5)

The voltammogram obtained is based on the theoretical Butler-Volmer equation, which is expressed as a function of the anode and cathode current:

$$I = I_0 [\exp(b_a(E_{app} - E_0)) - \exp(b_c(E_{app} - E_0))] \quad (\text{Eq 6})$$

Where b_a and b_c are the anodic and cathodic Tafel constants respectively, E_0 is the Nernst potential (V) and I_0 is the exchange current density (A g^{-1}) which are determined by the application of Stern's first rule to the voltammograms, $I = f(E_{app})$, gives us the Tafel curve, $\log I = f(E_{app})$

3. Result and discussion

3.1 Structural and morphological characterization of $\text{CaNi}_{4.8}\text{Mg}_{0.2}$ powders milled during 30, 40, 50, and 60h

3.1.1 Structural characterization

Fig. 1 shows the XRD diffractograms of the $\text{CaNi}_{4.8}\text{Mg}_{0.2}$ powder prepared by mechanosynthesis for different milling times (30, 40, 50, 60 h) with ball/powder weight ratio of 8:1.

These spectrums are refined using X'Pert High Score software. This refinement permitted us to identify the existig phases and to determine several parameters such as; the lattice parameters, the phase abundance, the average crystallite size and the quality of fit parameters in Table 1 (Ref 82).

Table 1 shows the various crystallographic parameters of the $\text{CaNi}_{4.8}\text{Mg}_{0.2}$ powders obtained for 30, 40, 50 and 60 h milling times.

At 30 h of milling (Fig. 1a), the XRD spectrum reveals the presence of two main phases Ni (cubic) and CaNi_5 (hexagonal) located, respectively, at the positions 51.98° , 60.8° , 91.40° and 24.74° , 36.75° , 42.92° , 51.99° , 57.23° . The peaks are broad and less intense compared to the peaks of the other samples which indicates the formation of an amorphous phase. The peaks of the initial elements Ca and Mg are not detected. Because, probably, a long milling time (30h) permitted to increase the temperature until reaching the melting temperature of Mg ($T=650^\circ\text{C}$), which means its complete melting and dissolution. With the increase of temperature, while passing by the melting temperature of Ca ($T=842^\circ\text{C}$), in the same manner, it will dissolve which explains the detection of nickel only ($T= 1455^\circ\text{C}$). The presence of the CaNi_5 phase is due to the dissolution of Ni atoms (atomic radius = 1.4\AA) in the Ca lattice (atomic radius = 1.8\AA) (Ref 83,50). When the milling time is extended to 40 h, The XRD spectrum (Fig. 1b) reveals the presence of the same main phases Ni (cubic) and CaNi_5 (hexagonal) located at 51.85° , 60.52° , 91.73° and 38.62° , 44.48° respectively. Showing an increase in intensities and the disappearance of some CaNi_5 peaks observed in 30 h. In the case of compounds ball-milled for 50 and 60 h (Fig. 1c and d), both CaNi_5 and Ni phases are still observed. There is a significant increase in the intensities with a reduction of the peak broadening, which can be

explained by the partial crystallization of the amorphous phase due to the increase of temperature during the time progression of the milling (Ref 51,28).

3.1.2 Morphological characterization

Fig. 2 shows the morphology and the EDX spectra of $\text{CaNi}_{4.8}\text{Mg}_{0.2}$ powders milled during 30, 40, 50, and 60h, before cycling with a ball/powder weight ratio of 8:1

This quantification is used to verify the formation of the solid solution and the homogeneity of the $\text{CaNi}_{4.8}\text{Mg}_{0.2}$ powders.

During 30 h milling time, the micrograph of the powder reveals the existence of agglomerates with an average particle size of 27 μm . This result is related to the cold-welding predominance of the milling process. By increasing the milling time to 40 h, the average particle size is about 22 μm . This decrease indicates that the milling process achieves a fracturing stage. During the milling times 50 and 60 h, the particle size continued to decrease to 22 and 20 μm respectively and the agglomerates gradually take on a rounded shape during the milling process (Ref 27,84, 85). These results show a general trend towards refinement and degradation of the coarse particles which are well combined with the structural results, which tend to reduce the diffraction peaks and increase the intensities according to the increase of milling time. According to the analysis of EDX spectra, all elements of Ca, Ni and Mg powders are present with chemical composition close to the nominal composition of $\text{CaNi}_{4.8}\text{Mg}_{0.2}$ powders (30, 40, 50, 60 h) (Table 2).

3.2 Electrochemical characterization of $\text{CaNi}_{4.8}\text{Mg}_{0.2}$ (30, 40, 50, and 60h) electrodes

3.2.1 Activation, cycling performance and polarization

Fig. 3 shows the evolution of discharge potential according to the electrochemical capacity, respectively, for $\text{CaNi}_{4.8}\text{Mg}_{0.2}$ electrode at different milling times: 30h, 40h, 50h and 60h.

In electrochemical cycling, metal compound activation is achieved if its discharge capacity reaches a maximum value, its half-discharge potential remains constant and its polarization becomes minimal (Ref 86). Usually, during the repetitive charge-discharge cycles, the negative electrode will be activated, i.e., it will be fragmented and cracked increasing then the active surface that facilitates the absorption and desorption of hydrogen. In another way, the rapid activation of the electrode shows its performance (Ref 87). The $\text{CaNi}_{4.8}\text{Mg}_{0.2}$ electrode at 30 h milling times is activated respectively during the 3rd cycle. Despite, the $\text{CaNi}_{4.8}\text{Mg}_{0.2}$ electrode milled during 40, 50 and 60h, needs only one cycle to be activated. Indeed, the maximum discharge capacities are about 118 mAhg^{-1} (3rd cycle), 87 mAhg^{-1} (1st cycle), 84 mAhg^{-1} (1st cycle) and 53 mAhg^{-1} (1st cycle), respectively for 30, 40, 50 and 60 h milling times.

Fig. 4 represents the evolution of the electrochemical discharge capacity as a function of the cycle number of the $\text{CaNi}_{4.8}\text{Mg}_{0.2}$ negative electrode at different milling times under a current of 0.7 mA in 6M KOH electrolyte.

After activation, the maximum discharge capacity decreases progressively with the cycles number, this decrease may be explained by a degradation of the active material of the electrode, by oxidation or dissolution, thus reducing the interstitial sites available for hydrogen insertion (Ref 88).

Table 3 shows the loss of the cycling capacity S_{50} at different milling times (30, 40, 50 and 60h) as $S_{50}(\%) = \left(\frac{C_{max} - C_{50}}{C_{max}} \right) * 100$, where C_{50} is the 50th discharge capacity cycle, C_{max} is the maximum discharge capacity.

It can be seen that the variation of the maximum discharge capacity has the same tendency as the stability cycles. With the increase of milling time from 30 to 60 hours, the discharge capacity drops from 118 to 53 mAh g^{-1} . It can be explained by the increase of the active surface area of

the compound according to the progress of milling time. As this increasing, the active surface becomes more exposed to the aggressive 6M KOH electrolyte, which accelerates its oxidation then the formation of an oxide layer, which explains the decrease in the discharge capacity (Ref 89). The poor discharge capacity and low stability of the $\text{CaNi}_{4.8}\text{Mg}_{0.2}$ compound at the 60h milling time is due to its amorphous structure because the amorphous alloy has a lower capacity than the others. Also, that can be related to the partial amorphous of the compound with increasing ball-milling time mentioned above (Ref 90).

The reversibility of the charging and the discharging reaction of the electrodes $\text{CaNi}_{4.8}\text{Mg}_{0.2}$ (30, 40, 50, and 60 h) deteriorates during cycling. Indeed, the $\text{CaNi}_{4.8}\text{Mg}_{0.2}$ polarization electrode increases progressively from 40, 168, 274, and 246 mV at the first cycle to 200, 259, 423, and 334 mV at the 50th cycle, respectively for 30 h, 40 h, 50 h, and 60 h milling times. This result is in good agreement with the decrease in the discharge capacity during cycling at different milling times. As a consequence, the good reversibility reaction of the $\text{CaNi}_{4.8}\text{Mg}_{0.2}$ electrode is obtained at the 30h time milling which is in good agreement with its electrochemical properties.

3.2.2 Kinetic parameters: current density and Nernst potential

Fig. 6 shows the evolution of some typical experimental and theoretical Tafel curves during cycling of $\text{CaNi}_{4.8}\text{Mg}_{0.2}$ electrode for different milling times (30, 40, 50 and 60 h), determined for a potential slow rate of 1 mV s^{-1} and 6M KOH concentration electrolyte.

The kinetic properties of $\text{CaNi}_{4.8}\text{Mg}_{0.2}$ (30, 40, 50, 60h) electrodes during long cycling performed by the potentiodynamic method (Ref 91,92). To study the kinetic properties, a linear potential of 1mVs^{-1} is applied to the negative electrode, then it should determine the

voltamogrammes, $I = f(E)$, after every five cycles of charge and discharge during a long cycling. The voltamograms obtained are processed by software based on Stern's first method to plot the potentiodynamic or Tafel polarisation curves, $\log|I| = f(E_{app})$.

During the first activation cycles, the Tafel curves move towards the positive potential where hydrogen insertion into the electrode has become increasingly easier. In fact, the values of the potential for the $\text{CaNi}_{4.8}\text{Mg}_{0.2}$ (30, 40, 50, 60 h) electrodes in the first cycle are about -921, -835, -842, -899 mV, respectively. While in 20th cycle, the potential value is about -915, -831, -812, -762 mV, respectively for the $\text{CaNi}_{4.8}\text{Mg}_{0.2}$ (30, 40, 50, 60 h) electrodes. After activation, the Tafel curves reverse their paths towards the less positive potential where the insertion of hydrogen into the electrode has become more difficult. Indeed, the values of the potential for the $\text{CaNi}_{4.8}\text{Mg}_{0.2}$ electrodes at the 25th cycle are about -918, -843, -813 and -795, while at the 50th cycle, are about -921, -837, -831, -767, for 30, 40, 50 and 60 h milling times, respectively. This result could be explained by the phenomenon of oxidation and dissolution of the active material of the electrode during electrochemical cycling. These results may be explained also by the phenomenon of electrode ageing due to the aggressivity of the 6M KOH electrolyte on the negative hydride electrode.

Fig. 7 shows the evolution of Nernst potential according to the cycle number of $\text{CaNi}_{4.8}\text{Mg}_{0.2}$ electrode determined at a current of 0.7 mA charge/discharge in 6M KOH electrolyte at different milling times (30, 40, 50 and 60 h).

The $\text{CaNi}_{4.8}\text{Mg}_{0.2}$ (60 h) electrode has a higher potential which is about -0.78V, this indicates that hydrogen insertion is easier at this milling time. This result is in good correlation with the cycling properties (activation, cycling resistance and polarization).

Fig. 8 shows the evolution of the exchange current density during cycling of the $\text{CaNi}_{4.8}\text{Mg}_{0.2}$ electrode, determined for a potential scan rate of 1 mV s^{-1} and 6M KOH electrolyte at different milling times (30, 40, 50, and 60 h).

The exchange current density at the 30h milling time, achieves its maximum values at the first activation cycles ($1827 \text{ mA} \cdot \text{g}^{-1}$), then gradually decrease progressively before stabilizing after the 40th cycle ($50 \text{ mA} \cdot \text{g}^{-1}$). At the other milling times (40, 50, and 60h), the exchange current density represents the same pattern with a high value of about $25 \text{ mA} \cdot \text{g}^{-1}$ at the activation cycles before stabilizing around minimum values ($\approx 10 \text{ mA} \cdot \text{g}^{-1}$).

3.3 Comparative study of the electrochemical properties of $\text{CaNi}_{4.8}\text{Mg}_{0.2}$ and negative electrodes for different milling times

Table 4 presents the different cycling parameters such as maximum discharge capacity, cycle stability, and degradation rate of the $\text{CaNi}_{4.8}\text{Mn}_{0.2}$ and $\text{CaNi}_{4.8}\text{Mg}_{0.2}$ negative electrodes for different milling times (30, 40, 50, 60 h) at 6M KOH electrolyte.

The discharge capacity C_{max} reaches a maximum value for a milling time of 30 h (118 mAhg^{-1}) and 40 h (96 mAhg^{-1}) respectively for $\text{CaNi}_{4.8}\text{Mg}_{0.2}$ and $\text{CaNi}_{4.8}\text{Mn}_{0.2}$ electrodes.

The largest loss of discharge capacity after the 50th cycle is observed for 50h and 60h milling times for both compounds $\text{CaNi}_{4.8}\text{Mn}_{0.2}$ and $\text{CaNi}_{4.8}\text{Mg}_{0.2}$.

Table 5 shows the polarization on activation of the $\text{CaNi}_{4.8}\text{Mn}_{0.2}$ and $\text{CaNi}_{4.8}\text{Mg}_{0.2}$ electrodes determined at a charge/discharge current of 0.7 mA in 6M KOH electrolyte at different milling times (30, 40, 50, and 60 h).

For $\text{CaNi}_{4.8}\text{Mn}_{0.2}$ electrode milled during 30h, the polarization is about 220 mV, then decreases slowly to 212 mV during 40h and 218 mV during 50h and finally it rises to 325 mV during 60h.

The reversibility of the charging and discharging reaction of the electrodes is better for the 40h milling time that agrees with its maximum discharge capacity value.

For the other electrode, the polarization is about 40 mV during the 30h milling time and then undergoes a remarkable increase to 168, 274 and 246 mV respectively for the 40, 50 and 60 h milling times. This shows that the best reversibility is obtained for the 30h electrode which is in good agreement with the other electrochemical results.

Table 6 shows the kinetic parameters of the $\text{CaNi}_{4.8}\text{Mn}_{0.2}$ and $\text{CaNi}_{4.8}\text{Mg}_{0.2}$ electrodes determined at a charge/discharge current of 0.7 mA in 6M KOH electrolyte at different milling times (30, 40, 50, and 60 h).

For $\text{CaNi}_{4.8}\text{Mn}_{0.2}$ compound, the Specific exchange current density reaches its maximum value of 83 mA g⁻¹ for 40 h milling time. For $\text{CaNi}_{4.8}\text{Mg}_{0.2}$ electrode reaches a maximum value for 30h milling time. These results are in good agreement with the previous results.

4. Conclusion

In this paper, structural, morphological and electrochemical properties of $\text{CaNi}_{4.8}\text{Mg}_{0.2}$ electrodes milled during 30, 40, 50 and 60h are presented using XRD, SEM and electrochemical methods (galvanostatic and potentiodynamic polarization).

The electrochemical study during activation and long cycling showed that:

- the $\text{CaNi}_{4.8}\text{Mg}_{0.2}$ (30, 40, 50, 60 h) electrodes activate respectively during the third, fourth and first cycle. Indeed, the discharge capacity values are 118, 87, 84 and 53 mAhg⁻¹.
- after activation, the discharge capacity decreases progressively during cycling, this decrease could be attributed to a degradation of the active material of the electrode.

- the $\text{CaNi}_{4.8}\text{Mg}_{0.2}$ (30 h) electrode has a good reversibility during the charge and discharge reaction than the other electrodes, which is in good agreement with its maximum discharge capacity and easy activation.
- the kinetic parameters of the $\text{CaNi}_{4.8}\text{Mg}_{0.2}$ (30 h) electrode show a good correlation with their electrochemical properties.

References

1. A. Ercetin, Application of the hot press method to produce new Mg alloys: Characterization, mechanical properties, and effect of Al addition, *J. Mater. Eng. Perform.*, 2021, 30(6), p 4254-4262
2. L. B. Lave, C. T. Hendrickson and F. C. McMichael, Environmental implications of electric cars, *Science*, 1995, 268, p 993–995
3. M. Menou, D. Ibrahim and R.A. Marc Review on use of phase change materials in battery thermal management for electric and hybrid electric vehicles., *Int. J. Energy Research*, 2016, 40 (8), p 1011-1031
4. C. Tarhan and M.A. Çil, A study on hydrogen, the clean energy of the future: Hydrogen storage methods, *J. Eng. Storage*, 2021, 40, p 102676
5. Y. Liu, H. Pan, M. Gao and Q. Wang, Advanced hydrogen storage alloys for Ni/MH rechargeable batteries, *J. Mater. Chem.*, 2011, 21, p 4743–4755
6. G.J. May, A. Davidson, and B. Monahov, Lead batteries for utility energy storage: A review, *J. Eng. Storage*, 2018, 15, p 145-157
7. E. Blumbergs, V. Serga, E. Platacis, M. Maiorov and A. Shishkin, Cadmium recovery from spent Ni-Cd batteries: a brief review, *Metals*, 2021, 11, p 1714

8. G. Genchi, M. S. Sinicropi, G. Lauria, A. Carocci and A. Catalano, The effects of cadmium toxicity, *Int. J. Environ. Res. Public. Health*, 2020,17, p 3782
9. W.B. Hawley and J. Li, Electrode manufacturing for lithium-ion batteries—Analysis of current and next generation processing, *J. Energy Storage*, 2019, 25, p 100862
10. C. Bibin, M. Vijayaram, V. Suriya, R.S. Ganesh and S. Soundarraj, A review on thermal issues in Li-ion battery and recent advancements in battery thermal management system, *Materials Today: Proceedings*, 2020,33, p 116-128
11. S. R. Ovshinsky and M. A. Fetcenko, Development of high catalytic activity disordered hydrogen-storage alloys for electrochemical application in nickel–metal hydride batterie, *Appl. Phys.*, 2001,72, p 239–244
12. J. Shin and J. W. Choi, Opportunities and reality of aqueous rechargeable batteries, *Adv. Energy Mater.*, 2020, 10(28), p 2001386
13. Y. B. Belgacem, C. Khaldi, J. Lamloumi and H. Takenouti, Effect of the discharge rate on the electrochemical properties of LaY₂Ni₉ hydrogen storage alloy, *J. Alloys Compd.*, 2015, 631, p 7–14
14. M.A. Fetcenko, S.R. Ovshinsky, B. Reichman, K. Young, C. Fierro, J. Koch, A. Zallen, W. Mays, T. Ouchi, Recent advances in NiMH battery technology, *J. Pow. Sou.*, 2007,165, p 544–551
15. X. Chen, A. Chu, D. Li, Y. Yuan, X. Fan and Y. Deng, Development of the cycling life model of Ni-MH power batteries for hybrid electric vehicles based on real-worldoperating conditions, *J. Energy Storage*, 2021, 34, p 101999
16. K. V. Vidyanandan, Batteries for electric vehicles, *Power Manag. Inst.*, 2019,20, p 38

17. M. Tliha, C. Khaldi, S. Boussami, N. Fenineche, O. ElKedim, H. Mathlouthi and J. Lamloumi, Kinetic and thermodynamic studies of hydrogen storage alloys as negative electrode materials for Ni/MH batteries: a review, *J. Solid State Electrochem.*, 2014, 18, p 577–593
18. G. H. Ağaoğlu and G. Orhan, Production and electrochemical characterization of MgNi alloys by molten salt electrolysis for Ni–MH batteries, *Int. J. Hydrog. Energy*, 2018,43, p 6266–6274
19. H. Inoue, T. Ueda, S. Nohara, N. Fujita and C. Iwakura, Effect of ball-milling on electrochemical and physicochemical characteristics of crystalline Mg₂Ni alloy, *Electrochimica Acta*, 1995,43, p 2215–2219
20. D. G. Oliva, M. Fuentes, E. M. Borzone, G. O. Meyer and P. A. Aguirre, Hydrogen storage on LaNi_{5-x}Sn_x, Experimental and phenomenological Model-based analysis, *Energy Convers. Manag.*, 2018,173, p 113–122
21. R.N. ELSHAER and K.M. IBRAHIM, Study of Microstructure, Mechanical Properties, and Corrosion Behavior of As-Cast Ni-Ti and Ti-6Al-4V Alloys. *J. Mater. Eng. Perform.*, 2022, p 1-15
22. M. Balcerzak, Structural, Electrochemical and Hydrogen Sorption Studies of Nanocrystalline Ti-V-Co and Ti-V-Ni-Co Alloys Synthesized by Mechanical Alloying Method. *J. Mater. Eng. Perform.*, 2019,28(8), p 4838-4844
23. H. Aoyagi, K. Aoki and T. Masumoto, Effect of ball milling on hydrogen absorption properties of FeTi, Mg₂Ni and LaNi₅, *J. Alloys Compd.*, 1995, 231, p 804–809
24. M. Pentimalli, F. Padella, L. Pilloni, E. Imperi and P. Matricardi, AB₅/AB₅ composite material for hydrogen storage, *Int. J. Hydrogen Energy*, 2009,34, p 4592–4596

25. M. Tousignant and J. Huot, Hydrogen sorption enhancement in cold rolled LaNi₅. *J. Alloys Compd.*, 2014,595, p 22–27
26. J. S. Benjamin, Dispersion strengthened superalloys by mechanical alloying, *Metall. Trans.*, 1970, 1, p 2943–2951
27. P.-Y. Lee, J.-L. Yang and H.-M. Lin, Amorphization behaviour in mechanically alloyed Ni—Ta powders, *Journal Mater. Sci.*, 1998, 33, p 235–239
28. C. Suryanarayana, Mechanical alloying and milling, *Prog. Mater. Sci.*, 2001, 46, p 1–184
29. P. G. Jamkhande, N. W. Ghule, A. H. Bamer and M. G. Kalaskar, Metal nanoparticles synthesis: An overview on methods of preparation, advantages and disadvantages, and application, *J. Drug Deliv. Sci. Technol.*, 2019,5, p 101174
30. J.B.v. Colbe, J.R.o Ares, J. Barale, M. Baricco, C. Buckley, G. Capurso, N. Gallandat, D.M. Grant, M.N. Guzik, I. Jacob, E.H. Jensen, T. Jensen, J. Jepsen, T. Klassen, M.V. Lototsky, K. Manickam, A. Montone, Puszkiel, S. Sartori, D.A. Sheppard, A. Stuart, G. Walker, C.J. Webb, H. Yang, V. Yartys, A. Zuttel and M. Dornheim, Application of hydrides in hydrogen storage and compression: Achievements, outlook and perspectives, *Int. J. Hydrog. Energy*, 2019, 44, p 7780–7808
31. A. El Kharbachi, E.M. Dematteis, K. Shinzato, S.C. Stevenson, L.J. Bannenberg, M. Heere and B.C. Hauback, Metal Hydrides and Related Materials, Energy Carriers for Novel Hydrogen and Electrochemical Storage, *J. Phys. Chem. C*, 2020, 124, p 7599-7607
32. U. Eberle, G. Arnold and R. Von Helmolt, Hydrogen storage in metal–hydrogen systems and their derivatives, *J. Power Sources*, 2006, 154, p 456–460

33. Y. Dabaki, C. Khaldi, O. ElKedim, N. Fenineche and J. Lamloumi, Phase structure and electrochemical characteristics of $\text{CaNi}_{4.7}\text{Mn}_{0.3}$ hydrogen storage alloy by mechanical alloying, *J. Solid State Electrochem.*, 2022, 26, p 457–468
34. W. Liao, W. Jiang, X.S. Yang, H. Wang, L. Ouyang and M. Zhu, Enhancing (de) hydrogenation kinetics properties of the Mg/MgH₂ system by adding ANi₅ (A = Ce, Nd, Pr, Sm, and Y) alloys via ball milling, *J. Rare Earths*, 2021, 39, p 1010-1016
35. Y. Ben Belgacem, C. Khaldi and J. Lamloumi, The effect of the discharge rate on the electrochemical properties of AB₃-type hydrogen storage alloy as anode in nickel-metal hydride batteries, *Int. J. Hydrogen Energy*, 2017, 42, p 12797-12807
36. M. Ayari, I. Sahli, M. Elghali, O. Ghodbane, H. Jaafar and M. Abdellaoui, Synthesis and characterizations of structural and electrochemical properties of $\text{CeTi}_2\text{Ni}_{4.5}\text{Al}_{0.2}\text{Mn}_{0.3}\text{Cr}_4$ AB₃ type compound, *J. Alloys and Comp.*, 2021, 884, p 161017
37. Y. Wu, Y. Peng, X. Jiang, H. Zeng, Z. Wang, J. Zheng and X. Li, Reversible hydrogenation of AB₂-type Zr–Mg–Ni–V based hydrogen storage alloys, *Progress in Natural Science: Mat. Int.*, 2021, 31, p 319–323
38. W. LI-MIN, H. RI, Effects of Long-Term Aging on Properties and Laves Phase Evolution of A New Type of Fe-Based Superalloy, *J. Mater. Eng. Perform.*, 2022, p. 1-11
39. B. Hosni, N. Fenineche, O. ElKedim, C. Khaldi and J. Lamloumi, Structural and electrochemical properties of TiFe alloys synthesized by ball milling for hydrogen storage, *J. Solid State Electrochem.*, 2018, 22, p 17–29
40. M. Marinelli and M. Santarelli, Hydrogen storage alloys for stationary applications, *J. Energy Storage*, 2020, 32, p 101864

41. M. Nowak, M. Balcerzak and M. Jurczyk, Effect of Substitutional Elements on the Thermodynamic and Electrochemical Properties of Mechanically Alloyed $\text{La}_{1.5}\text{Mg}_{0.5}\text{Ni}_{7-x}\text{M}_x$ alloys (M = Al, Mn), *Metals*, 2020, 10, p 578
42. A. DENG, Y. LUO, J. ZHOU, Y. Xie, Y. Yuan, X. Kang, H. Zhang, Effect of Mn Element on the Structures and Properties of A_2B_7 -Type La–Y–Ni-Based Hydrogen Storage Alloys, *Metals*, 2022, 12(7), p 1122
43. J.M. Joubert, M. Latroche and A.P. Guégan, Metallic Hydrides II: Materials for Electrochemical Storage, *MRS bulletin*, 2007, 27, p 694-698
44. W.L. Mi, Z.S. Liu, T. Kimura, A. Kamegawa and H.L Wang, Crystal structure and hydrogen storage properties of $(\text{La,Ce})\text{Ni}_{5-x}\text{M}_x$ (M = Al, Fe, or Co) alloys, *International Journal of Minerals, Metall. and Mat.*, 2019, 26, p 1-108
- 45 X. Chen, J. Xu, W. Zhang, S. Zhu, N. Zhang, D. Ke, J. Liu, K. Yan and H. Cheng, Effect of Mn on the long-term cycling performance of AB_5 -type hydrogen storage alloy, *Int. J. Hydrogen Energy*, 2021, 46, p 21973-21983
46. A. Singh, B.K. Singh, D.J. Davidson and O.N. Srivastava, Studies on improvement of hydrogen storage capacity of AB_5 type: $\text{MmNi}_{4.6}\text{Fe}_{0.4}$ alloy, *Int. J. Hydrogen Energy*, 2004, 29, p 1151 – 1156
47. F. Liang, J. Lin, Y. Chng, D. Yin, Y. Wu and L. Wang, Gaseous sorption and electrochemical properties of rare-earth hydrogen storage alloys and their representative applications: A review of recent progress, *Sci. China Technol. Sci.*, 2018, 61, p 1309–1318
48. Y. Liu, H. Pan, M. Gao and Q. Wang, Advanced hydrogen storage alloys for Ni/MH rechargeable batteries, *J. Mat. Chem.*, 2011, 21, p 4743-4755

49. J. Xu, X. Chen, W. Zhu, W. Zhang, H. Cui, S. Zhu and H. Cheng, Enhanced cycling stability and reduced hysteresis of AB₅-type hydrogen storage alloys by partial substitution of Sn for Ni, *Int. J. Hydrogen Energy*, 2022, 47(53), p 22495-22509
50. H. Zhang and L. Fu, Phase transformation relevant to the hydrogenation properties in the YNi_{3-x}Cr_x, *Chem. Phys. Lett.*, 2019, 736, p 136823
51. Y. Dabaki, C. Khaldi, N. Fenineche, O. ElKedim, M. Tliha and J. Lamloumi, Electrochemical Studies on the Ca-Based Hydrogen Storage Alloy for Different Milling Times, *Metal. and Mater. Int.*, 2021, 27, p 1005–1024
52. St. Todorova, V. Rangelova, L. Mihaylov and T. Spassov, Effect of hydrogen induced decrepitation on the hydrogen sorption properties of MmNi₅. *Int. J. Electrochem. Sci.*, 2020, 15, p 4900 – 4907
53. J. Czub, W. Jamka, J. Przewoznik, A. Zarzecka, A. Hoser, D. Wallacher, N. Grimm and L. Gondek, Structural peculiarities in the b phase of the La_{0.75}Ce_{0.25}Ni_{4.8}Al_{0.2} Deuterides, *J. Alloys and Compounds*, 2019, 788, p 533-540
54. E. Msika, M. Latroche, F. Cuevas and A.P. Guégan, Zr-substitution in LaNi₅-type hydride compound by room temperature ball milling, *Mater. Sci. Eng.*, 2004, 108, p 91–95
55. Y. Chen, C.A. Sequeira, X. Song, R. Neto and Q. Wang, Polytypism of La–Ni phases in multicomponent AB₅ type hydride electrode alloys, *Int. J. Hydrogen Energy*, 2002, 27, p 63-68
56. M.H. Mendelsohn, D.M. Gruen and A.E. Dwight, The effect of aluminium additions on the structural and hydrogen absorption properties of AB₅ Alloys with particular reference to the LaNi_{5-x}Al_x ternary alloy system, *J. The Less-Common Metals*, 1979, 63, p 193 – 207

57. D.G. Westlake, A geometric model for the stoichiometry and interstitial site occupancy in hybrids (deutrides) of LaNi_5 , LaNi_4Al and LaNi_4Mn , *J. the Less-Common Metals*, 1938, 91, p 275-292
58. M. Dymek, B. Rozdzyńska-Kielbik, V.V. Pavlyuk and H. Bala, Electrochemical hydrogenation properties of $\text{LaNi}_{4.6}\text{Zn}_{0.4-x}\text{Sn}_x$ alloys, *J alloys and Comp.*, 2015, 644, p 916–922
59. D.G. Olivaa, M. Fuentesaa, E.M. Borzoneb, G.O. Meyerb and P.A. Aguirrea, Hydrogen storage on $\text{LaNi}_{5-x}\text{Sn}_x$. Experimental and phenomenological Model-based analysis, *Eng. Conv. Manag.*, 2018, 173, p 113–122
60. S.K. Pandey, A. Srivastava and O.N. Srivastava, Improvement in hydrogen storage capacity in LaNi_5 through substitution of Ni by Fe, *Int. J. Hydrogen Energy*, 2007, 32, p 2461 – 2465
61. W.L. Mi, Z.S. Liu, T. Kimura, A. Kamegawa and H.L. Wang, Crystal structure and hydrogen storage properties of $(\text{La,Ce})\text{Ni}_{5-x}\text{M}_x$ (M = Al, Fe, or Co) alloys, *International Int. J. Min. Metall. Mat.*, 2019, 26, p 108-113
62. J.H. Van Vucht, F. Kuijpers and H.C. Bruning, Reversible room-temperature absorption of large quantities of hydrogen by intermetallic compounds, *Philips Res*, 1970, 25, p 133-140
63. J-M. Joubert, V. Paul-boncour, F. Cuevas, J. Zhang and M. Latroche, LaNi_5 related AB_5 compounds: structure, properties and applications, *J. Alloys and Compounds.*, 2021, 862, p 158163
64. J. Chen, S.X Dou and H.K Liu, Effect of partial substitution of La with Ce, Pr and Nd on the properties of LaNi_5 -based alloy electrodes, *J. Pow. Sourc*, 1996, 63, p 267-270
65. M. Ayari, V. Paul-Boncour, J. Lamloumi, H. Mathlouthi and A. Percheron-Guégan, Study of the structural, thermodynamic and electrochemical properties of

- LaNi_{3.55}Mn_{0.4}Al_{0.3}(Co_{1-x}Fe_x)_{0.75} (0 ≤ x ≤ 1) compounds used as negative electrode in Ni-MH batteries, *J. Alloys and Compounds*, 2006, 420, p 251–255
66. C. Khaldi, H. Mathlouthi, J. Lamloumi and A. Percheron-Guégan, Effect of partial substitution of Co with Fe on the properties of LaNi_{3.55}Mn_{0.4}Al_{0.3}Co_{0.75-x}Fe_x (x=0.50, 0.15, 0.55) alloys electrodes, *J. Alloys Compd.*, 2003, 360, p 266–271
67. A. Merzouki, C. Cachet-Vivier, V. Vivier, J.-Y. Nédélec, L.T. Yub, N. Haddaoui, J.-M. Joubert and A. Percheron-Guégan, Microelectrochemistry study of metal-hydride battery materials Cycling behavior of LaNi_{3.55}Mn_{0.4}Al_{0.3}Co_{0.75} compared with LaNi₅ and its mono-substituted derivative, *J. Power Sources*, 2002, 109, p 281–286
68. Z.P. Li and S. Suda, A new family of hydride electrode materials based on CaNi₅-type Alloys, *J. Alloys Compd.*, 1995, 231, p 751-754
69. P.D. Goodell, Stability of rechargeable hydriding alloys during extended cycling, *J. Less-Common Metals*, 1984, 99, p 1–14
70. J.O. Jensen and N.J. Bjerrum, Systematic B-metal substitution in CaNi₅, *J. Alloys Compd.*, 1995, 293-295, p 185–189
71. K. Hong, The development of hydrogen storage electrode alloys for nickel hydride batteries, *J. Power Sources*, 2001, 96, p 85-89
72. G. Liang, S. Ruggeri, C. Lenain, H. Alamdari, J. Huot, L. Roue and R. Schulz, Synthesis of nanocrystalline CaNi₅-Based alloys and use for metal hydride electrode, *Mater. Sci. for*, 2001, 377, p 71-76
73. S. Chumphongphan, M. Paskevicius, D.E. Sheppard and C.E. Buckley, Effect of Al and Mo substitution on the structural and hydrogen storage properties of CaNi₅. *Int. J. Hydrogen Energy*, 2013, 38, p 2325-2331

74. Y. Dabaki, C. Khaldi, O. ElKedim, N. Fenineche and J. Lamloumi, Structural, morphological, and electrochemical properties of AB₅ hydrogen storage alloy by mechanical alloying, *Env. Prog. Sust. Energy*, 2021, 41, p 13739
75. Y. Dabaki, C. Khaldi, O. ElKedim, N. Fenineche and J. Lamloumi, Electrochemical properties of the CaNi_{5-x}Mn_x electrodes synthesized by mechanical alloying, *Int. J. Energy Research*, 2020, 44, p 10112-10125
76. P.S. Gilman and J.S. Benjamin, Mechanical alloying, *Ann. Rev. Mater. Sci.*, 1938, 13, p 279-300
77. I. Karaoud, Y. Dabaki, C. Khaldi, O. ElKedim, N. Fenineche and J. Lamloumi, Electrochemical properties of the CaNi_{4.8}M_{0.2}(M=Mg, Zn, and Mn) mechanical milling alloys used as anode materials in nickel-metal hydride batteries, *Env. Prog. Sust. Energy*, 2023, p 14118
78. J.S. Benjamin, Mechanical Alloying. A Perspective, *Metal Powder Rep.*, 1990, 45, p 122-127
79. M. Geng, J. Han, F. Feng and D.O. Northwood, Charging/discharging stability of a metal hydride battery electrode, *J. Electrochem. Soc.*, 1999, 146, p 2371
80. W. Zayani, S. Azizi, M. Salah, K.S. El-Nasser, I. Othman Ali and J. Lamloumi, Structure and electrochemical hydrogen storage properties of spinel ferrites Sm_xZn_{1-x}Fe₂O₄ alloys (x = 0, x = 0.2, x = 0.4, and x = 0.6) for Ni-MH accumulator applications, *Env. Prog. Sust. Energy*, 2022, p 14050
81. Y. Ben Belgacem, C. Khaldi, J. Lamloumi and H. Takenouti, The electrochemical performance of AB₃-type hydrogen storage alloy as anode material for the nickel metal hydride accumulators, *J. Solid State Electrochem.*, 2016, 20, p 1949–1959

82. H. Rietveld, Line profiles of neutron powder-diffraction peaks for structure refinement. *Acta Crystallogr.*, 1967, 22, p 151–152
83. H. Rietveld, A profile refinement method for nuclear and magnetic structures, *J Appl Crystallogr.*, 1969, 2, p 65-71
84. C. Suryanarayana, Mechanical alloying and milling, *Progress in Materials Science*, 2001, 46, p 1-184
85. H. Ahn, H.S. Shin, Y.J. Kim and H. Chung, Structural modification of carbon nanotubes by various ball milling, *J. Alloys Compd*, 2007, 434, p 428-432
86. C. Khaldi, H. Mathlouthi and J. Lamloumi, A comparative study of 1M and 8M KOH electrolyte concentrations, used in Ni–MH batteries, *J. Alloys and Compd*, 2009, 469, p 464–471
87. B. Liu, M. Hu, Y. Zhou, A. Li, L. Ji, Y. Fan and Z. Zhang, Microstructures and electrochemical characteristics of $\text{La}_{0.7}\text{Ce}_{0.3}\text{Ni}_{3.75-x}\text{Cu}_{0.75}\text{Mn}_{0.35}\text{Al}_{0.15}(\text{V}_{0.81}\text{Fe}_{0.19})_x$ ($x=0-0.20$) hydrogen storage alloys, *J. Alloys Compd.*, 2012, 544, p 105-110
88. W. Zayani, S. Azizi, K.S. El-Nasser, I. Othman Ali, M. Molière, N. Fenineche, H. Mathlouthi and J. Lamloumi, Electrochemical behavior of a spinel zinc ferrite alloy obtained by a simple sol-gel route for Ni-MH battery applications, *Int. J. Energy Research*, 2021, 45, p 5235–5247
89. Y. Dabaki, S. Boussami, C. Khaldi, H. Takenouti, O. ElKedim, N. Fenineche and J. Lamloumi, The effect of ZnO addition on the electrochemical properties of the $\text{LaNi}_{3.55}\text{Mn}_{0.4}\text{Al}_{0.3}\text{Co}_{0.2}\text{Fe}_{0.55}$ electrode used in nickel–metal hydride batteries, *J. Solid State Electroch.*, 2017, 21, p 1157-1164

90. H.L. Chu, S.J. Qiu, Q.F. Tian, L.X. Sun, Y. Zhang, F. Xu, Y.Y. Liu, Y.N. Qi and M.Q. Fan, Effect of ball-milling time on the electrochemical properties of La–Mg–Ni-based hydrogen storage composite alloys, *Int. J. Hydrogen Energy*, 2007, 32, p 4925 – 4932
91. C. Khaldi, S. Boussami, M. Tliha, S. Azizi, N. Fenineche, O. ElKedim, H. Mathlouthi and J. Lamloumi, The effect of the temperature on the electrochemical properties of the hydrogen storage alloy for nickel–metal hydride accumulators, *J. Alloys Compd.*, 2013, 574, p 59–66
92. R. Dahsa, M. Dymek, Y. B. Belgacem, J. Lamloumi, C. Khaldi and H. Bala, Determination of H₂O/H₂ system exchange current densities on cycled hydride electrodes from overswitch potential jump at low and high charge/discharge rates, *Int. J. Hydrogen Energy*, 2023, 48, p 15203-15214